Journal of Materials Science & Technology 72 (2021) 189–196

Contents lists available at ScienceDirect

Journal of Materials Science & Technology

journal homepage: www.jmst.org

Research Article

Patterned growth of β-Ga_2O_3 thin films for solar-blind deep-ultraviolet photodetectors array and optical imaging application

Chao Xie [a], Xingtong Lu [a], Yi Liang [a], Huahan Chen [a], Li Wang [a], Chunyan Wu [a], Di Wu [b], Wenhua Yang [a], Linbao Luo [a,*]

[a] School of Electronic Science and Applied Physics, Hefei University of Technology, Hefei, 230009, China
[b] School of Physics and Microelectronics, Zhengzhou University, Zhengzhou, 450052, China

ARTICLE INFO

Article history:
Available online 28 September 2020

Keywords:
Ultrawide-bandgap semiconductor
Solar-blind
Deep ultraviolet photodetection
Patterned growth
Image sensor

ABSTRACT

Solar-blind deep-ultraviolet (DUV) photodetectors based on Ga_2O_3 have attracted great attention due to their potential applications for many military and civil purposes. However, the development of device integration for optoelectronic system applications remains a huge challenge. Herein, we report a facile method for patterned-growth of high-quality β-Ga_2O_3 thin films, which are assembled into a photodetectors array comprising 8 × 8 device units. A representative detector exhibits outstanding photoresponse performance, in terms of an ultra-low dark current of ~0.62 pA, a large I_{light}/I_{dark} ratio exceeding 10^4, a high responsivity of ~0.72 A W^{-1} and a decent specific detectivity of ~4.18 × 10^{11} Jones, upon 265 nm DUV illumination. What is more, the DUV/visible (250/400 nm) rejection ratio is as high as 10^3 with a sharp response cut-off wavelength at ~280 nm. Further optoelectronic analysis reveals that the photodetectors array has good uniformity and repeatability, endowing it the capability to serve as a reliable DUV light image sensor with a decent spatial resolution. These results suggest that the proposed technique offers an effective avenue for patterned growth of β-Ga_2O_3 thin films for multifunctional DUV optoelectronic applications.

Introduction

Solar-blind deep-ultraviolet (DUV) spectrum regime refers to the solar radiation with wavelength of 200–280 nm, which does not exist at the surface of the Earth because of the strong absorption of ozone and atmosphere layers [1,2]. Photodetectors operating in this waveband region with a response cut-off wavelength around or below 280 nm are named as solar-blind photodetectors, which have pivotal applications in a variety of military and civil areas including missile guidance systems, intersatellite communication, flame detection, biochemical detection and remote control, etc [3,4]. Holding apparent advantages such as large bandgaps significantly exceeding the 3.4 eV of GaN, intrinsic solar-blindness and high radiation hardness, ultra-wide bandgap (UWBG) semiconductors including $Al_xGa_{1-x}N$, BN, $Zn_xMg_{1-x}O$, gallium oxide (Ga_2O_3) and diamond are promising candidates for solar-blind DUV photodetection, and have also been extensively explored in recent years [2,5,6]. Among them, monoclinic Ga_2O_3 (β-Ga_2O_3), which is the most stable form of Ga_2O_3 under normal conditions, has a direct bandgap ranging from 4.4-5.1 eV, corresponding to an absorption cut-off wavelength in the range of 240–280 nm [7]. Such an optical property enables photodetection over the full region of solar-blind DUV. Moreover, this kind of material exhibits high thermal and chemical stabilities [8]. The above characteristics make β-Ga_2O_3 extremely attractive for developing solar-blind DUV photodetectors, in particular, with the purpose for use in some high-temperature or harsh environments [9,10]. So far, a large number of high-performance DUV photodetectors composed of β-Ga_2O_3 in bulk, thin film or nanostructure forms have been reported [11–17]. Different device geometries including photoconductors [13], metal-semiconductor-metal (MSM) photodetectors [18], heterojunction/Schottky barrier photodiodes [19–21], and avalanche photodiodes [22,23] have also been involved. Among these, MSM photodetectors based on β-Ga_2O_3 thin films are of particular interest due to a range of features such as mature material preparation techniques, simple device fabrication, low dark current, the potential to attain high photogains with large responsivities, the good homogeneity of the material for easy integration with readout circuity, etc [24].

* Corresponding author.
E-mail address: luolb@hfut.edu.cn (L. Luo).

https://doi.org/10.1016/j.jmst.2020.09.015
1005-0302/

By far, β-Ga_2O_3 thin film-based MSM photodetectors in the form of individual device unit have been widely studied [2,11]. Most recently, several research groups have presented two-dimensional (2D) or even three-dimensional (3D) photodetectors array based on monolithic β-Ga_2O_3 thin films that exhibit outstanding DUV photoresponse with good device uniformity. [24–26] In addition, preliminary device integration technique towards multifunctional optoelectronic applications such as DUV image sensing, multipoint light spatial distribution recognition and real-time light trajectory has also been successfully developed. From the perspective of device fabrication, these applications often involve the patterning of β-Ga_2O_3 thin films by a controlled etching process, which is essentially required to achieve intra-device isolation and depress crosstalk between adjacent devices [7]. Thin films of β-Ga_2O_3 are normally grown on sapphire substrates via synthetic methods such as molecular beam epitaxy (MBE), metalorganic chemical vapor deposition (MOCVD), magnetron sputtering and so on [27,28]. To attain a good crystalline quality, high temperature is usually involved in the preparation process, which precludes the possibility of pre-patterning the material assisted by a photolithography process [29–31]. On the other hand, etching is also problematic for β-Ga_2O_3 material due to the difficulties such as isotropic etching and surface dangling bonds-dependent etching properties in wet etching, as well as low etching rate, poor surface morphology and introduction of ion-induced damage in dry etching [7,32,33].

Herein, we present a technique combing procedures of standard ultraviolet (UV) photolithography, metal deposition and thermal-assisted conversion, for patterned growth of β-Ga_2O_3 thin films with high crystalline quality. Via this method, MSM photodetectors array composed of 8 × 8 device units are realized, which displays not only a good photoresponse to DUV irradiation but also a narrow unit-to-unit variation. The important performance parameters including dark current, I_{light}/I_{dark} ratio, responsivity and specific detectivity attain ~0.62 pA, ~6.13×10^4, ~0.72 A W^{-1} and ~4.18×10^{11} Jones, respectively, at 265 nm DUV illumination. In addition, the detectors also display a steep response cut-off wavelength at around 280 nm with the DUV/visible (250/400 nm) rejection ratio exceeding 10^3. Furthermore, the present patterned photodetectors array also shows the capability to serve as a DUV light image sensor with satisfying resolution. It is believed that our study provides a facile, reliable and low-cost pathway for patterned growth of high-quality β-Ga_2O_3 thin films towards device integration for multifunctional DUV optoelectronic application purposes.

Experimental

Material preparation and characterization

The patterned β-Ga_2O_3 thin films were prepared by using a method containing standard ultraviolet (UV) photolithography, metal deposition and thermal-assisted conversion processes. A SiO_2/Si substrate was ultrasonically cleaned sequentially in acetone, ethanol and deionized water for 10 min, respectively, and dried in a flow of N_2 gas prior to use. The substrate was then spin-coated with a solution of positive photoresist, and a standard UV photolithography process was performed, which defined the photoresist layer with designed patterns. Afterwards, Ga layer with a thickness of ~22 nm was deposited onto the substrate in an ultrahigh vacuum chamber via thermal evaporation of metallic Ga (Aldrich, 99.99 %). After a lift-off process, patterned Ga thin films was formed on the substrate. Subsequently, the substrate was transferred into a horizontal tube furnace. After evacuation, a constant flow of O_2 gas (50 sccm) was introduced through the tube, and the tube pressure was maintained at 50 mTorr. The furnace was then heated to 1100 °C and kept at this temperature for 1 h to conduct the thermal-assisted conversion. After reaction, the furnace was cooled down naturally, and the patterned β-Ga_2O_3 thin films were obtained on the substrate.

The morphology and composition of the as-prepared β-Ga_2O_3 thin films were studied by a field-emission scanning electron microscope (FESEM, Quanta, FEG 250) equipped with an energy-dispersive spectrometer, and X-ray diffraction (XRD, X'Pert PRO MPD). The absorption spectrum was recorded on a CARY 5000 UV–vis (NIR) spectrophotometer. The X-ray photoelectron spectroscopy (XPS) measurement was performed by using a monochromatic Al *K*α source produced by the XPS system (Thermo ESCALAB250 X-ray photoelectron spectroscopy).

Device fabrication and analysis

The β-Ga_2O_3 thin film-based photodetectors array was constructed following the procedures as schematically shown in Fig. 1. β-Ga_2O_3 thin films with the pattern of an 8 × 8 squares array was first obtained on a cleaned SiO_2/Si substrate by using the method described above. The size of an individual square pattern is 300 μm × 300 μm. Then, Au electrodes (50 nm) array with a channel length of 45 μm was deposited by another UV photolithography, electron beam deposition and lift-off processes. The electrical properties was characterized by using a semiconductor parameter analyzer (Keithley 4200-SCS) on a probe station. A UV light-emitting diode (LED) with the wavelength of 265 nm (Thorlabs M265L3) serving as the light source was used to study the photoresponse performance. For spectral response study, a lab-built optoelectronic system consisting of a light source (LE-SP-LS-XE) and monochromator (LE-SP-M300) was employed. Before use, the intensity of all light sources was carefully calibrated by using a power meter (Thorlabs GmbH., PM 100D). All measurements were carried out in air at room temperature.

Results and discussion

In this work, the patterned β-Ga_2O_3 thin films were prepared through a thermal-assisted conversion method, as schematically shown in Fig. 1. The detailed procedures can be found in the "Experimental Section". First, a standard UV photolithography was carried out to define a photoresist layer on a cleaned SiO_2/Si substrate with predesigned patterns. Then, the patterned Ga thin films were obtained on the substrate through thermal evaporation, followed by a lift-off process. Finally, β-Ga_2O_3 thin films with patterns were formed by transferring the substrate into a tube furnace, where a thermal-assisted conversion process was conducted. To fabricate the β-Ga_2O_3 thin film-based photodetectors array, another procedure containing UV photolithography, Au deposition via electron-beam evaporation and lift-off was then performed.

The morphological and structural characterizations were carried out to study the quality of the as-grown patterned β-Ga_2O_3 thin films. Fig. 2(a)-(c) illustrates the FESEM images of β-Ga_2O_3 thin films of periodic square array, round array and triangle array. Apparently, these films exhibited uniform and regular shapes with desired patterns, implying the successful patterned growth of β-Ga_2O_3 thin films with the proposed technique. As observed from a magnified FESEM image (insert in Fig. 2(b)), the β-Ga_2O_3 thin films were virtually composed of closely compact crystalline grains with size of ~100 nm, similar to those β-Ga_2O_3 thin films grown by plasma enhanced chemical vapor deposition (PECVD) technique [20]. In addition to the above patterns, our technique could also be applied to grow β-Ga_2O_3 thin films with other patterns. As shown in Fig. 2(d), stripe patterns with a gap width of 10 μm were realized, and even with the stripe width of only 4 μm, continuous and regular stripes of β-Ga_2O_3 thin film with sharp edges could still

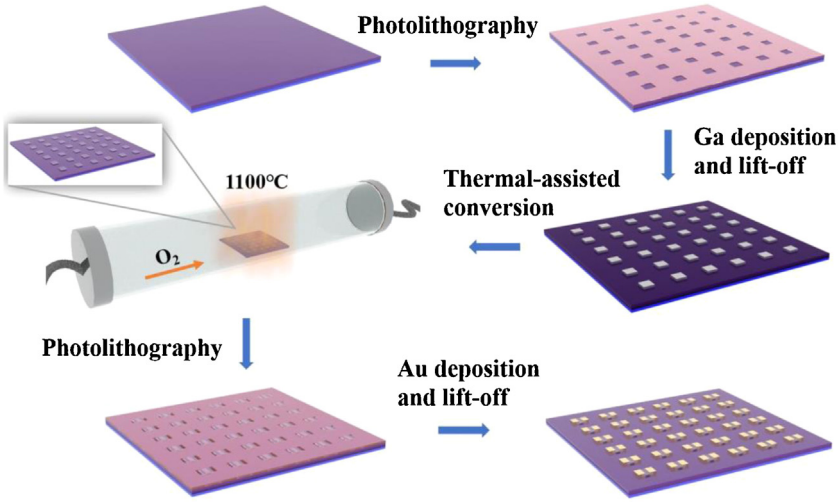

Fig. 1. Schematic illustration of the procedures for fabricating patterned β-Ga_2O_3 thin film-based photodetectors array.

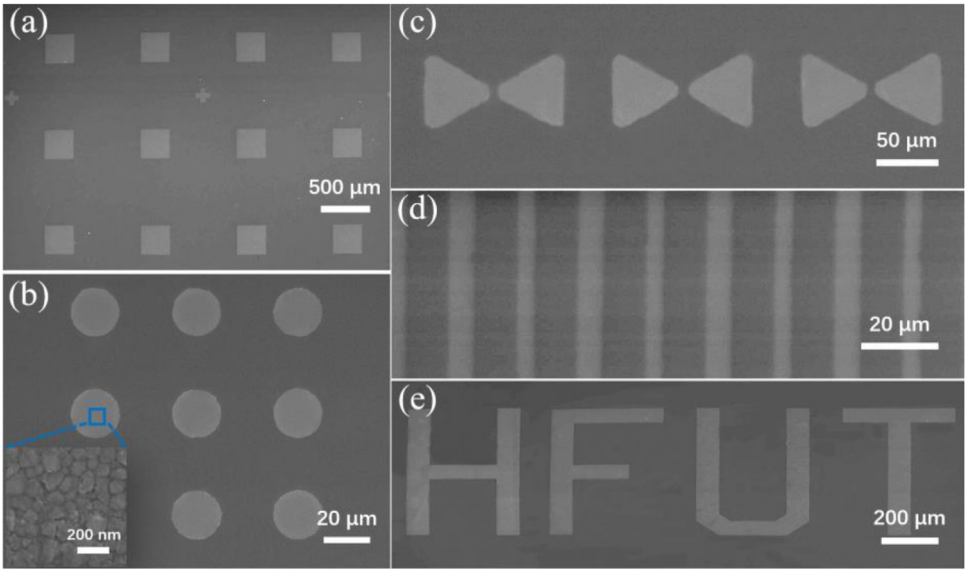

Fig. 2. FESEM images of the β-Ga_2O_3 thin films with the patterns of (a) periodic square array, (b) periodic round array, (c) periodic triangle array, (d) continuous 4 and 6 μm stripes and (e) "HFUT" characters. Inset in (b) shows an enlarged FESEM image of the β-Ga_2O_3 thin film.

be obtained. Moreover, Fig. 2(e) displays a FESEM image of patterned β-Ga_2O_3 thin films arranged in a shape of "HFUT" character. Besides, it should be mentioned that un-patterned β-Ga_2O_3 thin films in a large scale could also be grown using our method without the process of UV photolithography (Fig. S1 in Supporting Information). These results suggested that the proposed technique held high maneuverability and was scalable for growing β-Ga_2O_3 thin films with more complicated patterns towards multiple applications.

Fig. 3(a) depicts the X-ray energy-dispersive spectrometer (EDS) profile of the as-prepared thin films, from which the atomic ratio of Ga:O was determined to be 42.63:57.37. This value was in good accordance with the result obtained from XPS analysis (Fig. S2 in Supporting Information), and was close to the stoichiometric ratio of Ga_2O_3 as well. The XRD pattern plotted in Fig. 3(b) displays several evident peaks, which could be readily assigned to the β-Ga_2O_3 (JCPDS card No. 43-1012) [15]. Furthermore, from the optical absorption spectrum of the films (Fig. 3(c)), pronounced absorption at the DUV wavelength regime ranging from 200 to 280 nm along with a steep absorption cut-off edge situated at ~280 nm was found. Additionally, the optical bandgap was deduced to be ~5.15 eV from the curve of $(\alpha h\nu)^2$-$h\nu$ (where α, h and ν denote absorbance, Planck's constant and frequency, respectively), which agreed well the reported values in literatures [2,7]. Therefore, by using this method, high-quality β-Ga_2O_3 thin films can be successfully prepared.

With the patterned β-Ga_2O_3 thin films as the building blocks, a photodetectors array composed of 8 × 8 devices pixels was constructed. Fig. 3(d) depicts a FESEM image of a representative photodetector with a typical MSM device geometry. The elemental mapping profiles shown in Fig. 3(e) and (f) revealed clear and regular distribution boundaries of Au and Ga elements. Some unwanted Ga element detected beyond the region of the β-Ga_2O_3 thin film is probably caused by the residues during the lift-off process, which could be avoided by optimizing the experimental conditions in future work.

The optoelectrical properties of the as-synthesized β-Ga_2O_3 thin films were then characterized in order to study their potential application in deep-ultraviolet detector. Fig. 4(a) compares the current-voltage (*I-V*) curves of a typical photodetector in dark and

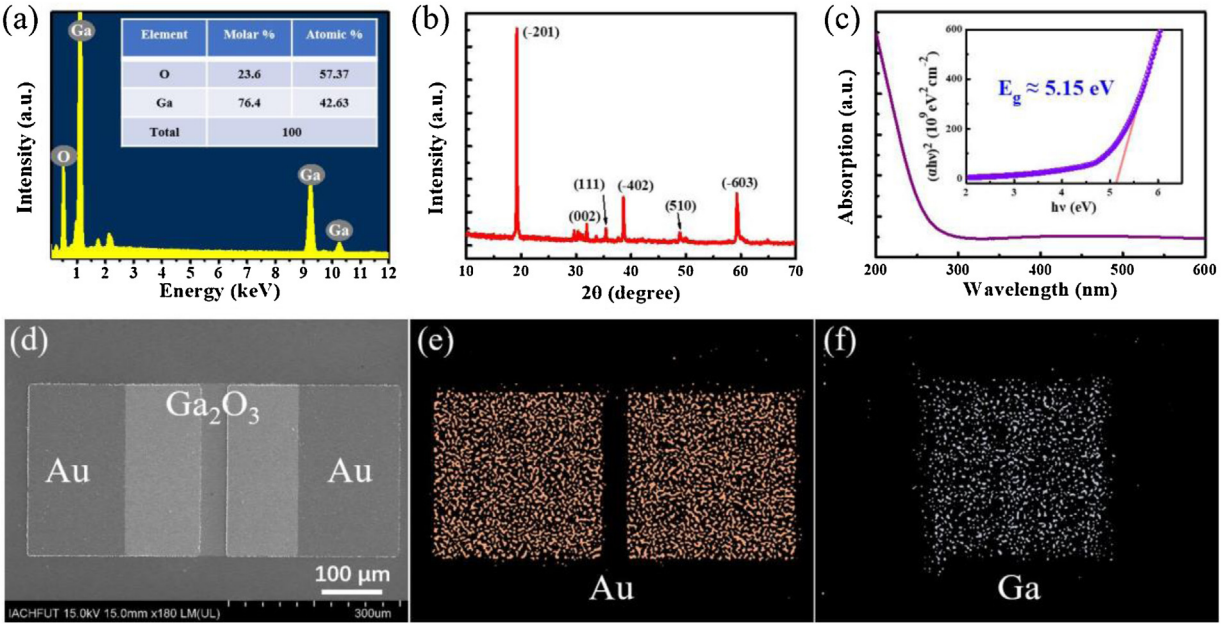

Fig. 3. (a) EDS spectrum and chemical composition of both gallium and oxygen atoms, (b) XRD pattern and (c) absorption spectrum of the β-Ga_2O_3 thin film, the inset in (c) shows the plot of $(\alpha h\nu)^2$-$h\nu$ for deducing the optical bandgap of the β-Ga_2O_3 thin film. (d) FESEM image of a typical β-Ga_2O_3 thin film-based photodetector with a MSM geometry. The elemental mapping showing the distribution of (e) Au and (f) Ga elements.

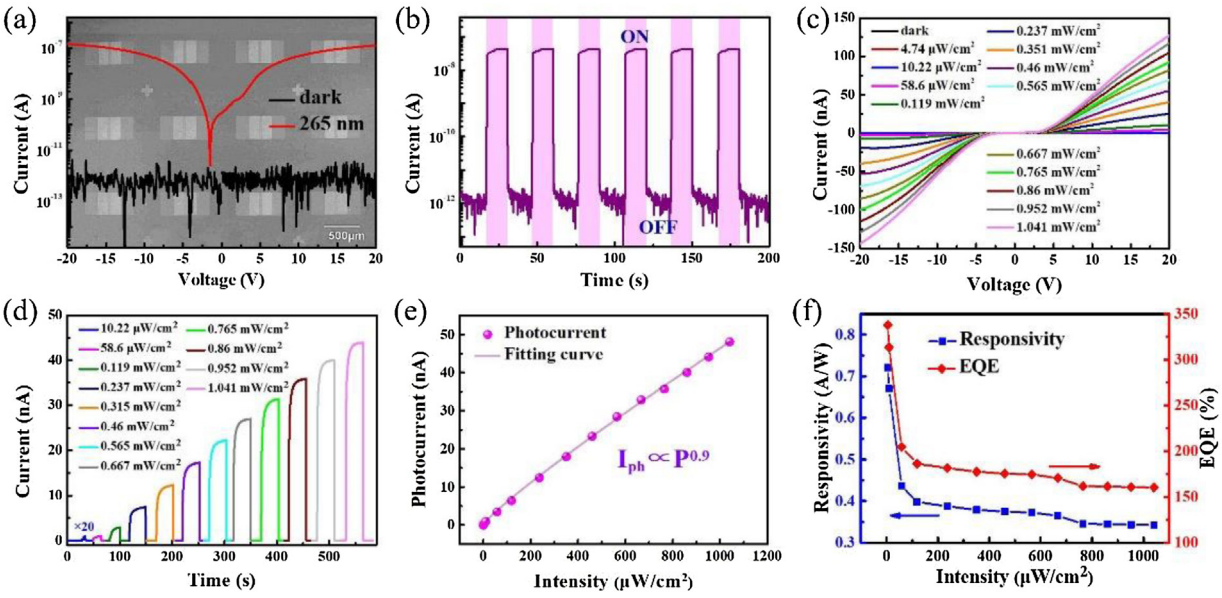

Fig. 4. (a) *I-V* curves of the β-Ga_2O_3 thin film-based photodetector in dark and under 265 nm illumination (0.952 mW cm^{-2}). The background is a FESEM image of the photodetectors array. (b) Time-dependent photoresponse of the device under 265 nm illumination. (c) *I-V* curves and (d) time-dependent photoresponse of the device under 265 nm illumination with different light intensities. (e) Photocurrent and (f) responsivity and EQE of the device as functions of light intensity.

under 265 nm DUV irradiation with a light intensity of 0.952 mW cm^{-2}. Evidently, the device had an extremely low dark current on the order of only pA even at a bias voltage of 20 V. It should be noted that the dark current was in fact over-valuated due to the limitations of our measurement conditions and instruments, considering that the measured dark current kept almost invariant within a large operational bias voltage range from -20 to 20 V in spite of some fluctuations. Interestingly, the channel current increased drastically by more than 4 orders of magnitude at 20 V when shinned by the DUV illumination, giving rise to a pronounced photoresponse. Furthermore, the time-dependent photoresponse was studied under the periodically turned DUV irradiation. As displayed in Fig. 4(b), the channel current could be readily switched between low- and high-value states with excellent repeatability, indicating a good optical switching characteristic. At a bias of 10 V, the average values of dark current and photocurrent were ~6.2×10^{-13} A and ~3.8×10^{-8} A, respectively, which rendered a large I_{light}/I_{dark} ratio as high as ~6.13×10^4.

The above photoresponse depended significantly on the incident DUV light intensity. Fig. 4(c) demonstrates the *I-V* characteristics upon the DUV illumination with different light intensities in the range of 4.74 μW cm^{-2} - 0.565 mW cm^{-2}. Apparently, the current rose gradually at both positive and negative bias voltages as the light intensity increased. Further study of time-dependent photoresponse under periodically switched DUV illumination with varied intensities also revealed an identical evolution tendency

Table 1
Comparison of some key performance parameters of our device and β-Ga_2O_3 thin film-based DUV photodetectors in literatures.

Method	Dark current (*A*)	I_{light}/I_{dark} ratio	Responsivity (A W^{-1})	D^* (Jones)	τ_r/τ_d (s)	Ref.
PLD	1.88×10^{-7}	~10	7.1 (10 V)	–	–	[38]
magnetron sputtering	7.63×10^{-9}	1.08×10^3	2.6 (10 V)	1.6×10^{12}	0.26/1	[37]
magnetron sputtering	1.0×10^{-11}	$\sim 10^5$	0.89 (10 V)	–	0.3/0.25	[24]
PECVD[a]	4.0×10^{-10}	37	2.0×10^{-4} (0 V)	6.9×10^9	–	[20]
PECVD	4.0×10^{-10}	$\sim 10^5$	1.2 (10 V)	1.9×10^{12}	–	[25]
OFZ[b]	2.3×10^{-10}	$\sim 10^2$	4 (40 V)	–	0.3/0.2	[40]
Thermal-assisted conversion	6.2×10^{-13}	6.13×10^4	0.72 (10 V)	4.18×10^{11}	1.1/0.03	This work

[a] Plasma-enhanced chemical vapor deposition; [b] Optical float-zone.

(Fig. 4(d)). This kind of relationship was reasonable because more photoinduced electron-hole pairs would be generated under the light irradiation with a higher intensity, which contributed to a larger photocurrent. In addition, we also noted that the β-Ga_2O_3 thin film-based detector could exhibit good optical switching feature for all illuminating conditions (Fig. 4(d)), suggesting that it could operate properly upon the DUV illuminations in a broad intensity regime. To gain more understanding of the above relationship, the dependence of photocurrent at 10 V on the light intensity was then fitted by using an extensively employed power law: $I_{ph} \propto P^{\theta}$, where I_{ph} and P represent the net photocurrent (I_{ph}=I_{light}-I_{dark}) and the light intensity, and the index θ is an empirical value reflecting the photocarrier recombination activity [34]. By carefully fitting the curve, a θ = 0.9 was attained in the light intensity of 10.22 μW cm^{-2} - 1.041 mW cm^{-2} (Fig. 4(e)). The slight deviation from the ideal value (θ = 1) suggested the existence of photocurrent recombination loss in the device, which was likely due to the presence of some trap states between the Fermi level and the conduction band edge [35].

In order to compare the performance of varied DUV photodetectors more equitably, we then calculated several pivotal performance parameters including responsivity (R) and external quantum efficiency (EQE). These two parameters are usually described by the following formula: [36]

$$R = \frac{I_{ph}}{P_{\lambda} S} = \mathrm{EQE}\left(\frac{e\lambda}{hc}\right) \quad (1)$$

where P_{λ}, S, e, λ, h, and c denote the light intensity, the effective illumination area (S = 1.35 × 10^{-4} cm^2, the S equals to the channel area, which is determined by multiplying the channel length (~45 μm) by the channel width (~300 μm), the basic electronic charge (1.6 × 10^{-19} C), the incident light wavelength, the Planck's constant and the speed of light, respectively. Therefore, the values of R and EQE were determined to be ~0.72 A W^{-1} and ~338 %, respectively, at the light intensity of 4.74 μW cm^{-2}. Although the R value was slightly lower than that of DUV photodetectors based on β-Ga_2O_3 thin films prepared via physical vapor deposition (PVD) methods including magnetron sputtering and pulsed laser deposition (PLD) (0.89–7.1 A W^{-1}) [24,37,38], it was still higher than that of devices comprising β-Ga_2O_3 thin films grown by MOCVD and low pressure chemical vapor deposition (LPCVD) techniques (0.32 mA W^{-1}-0.14 A W^{-1}) [9,39]. The R and EQE could be further improved by optimizing the device geometry, for example, shrinking the device channel width or employing interdigitated electrodes. In addition, it was found that both R and EQE values decreased monotonously with the increase in the light intensity. The results again verified that photocurrent recombination loss presented in the current device and could be ascribed to the intensified activity of photocarrier recombination due to increased density of charge carriers in the thin film when shinned by light illumination with a higher intensity.

Besides, specific detectivity (D^*) is also one of the key figure-of-merits of a photodetector, which is usually employed to describe the smallest detectable signal. This parameter can be expressed by the following equations [2,16]:

$$D^* = \frac{(AB)^{1/2}}{\mathrm{NEP}} \quad (2)$$

$$\mathrm{NEP} = \frac{i_n^{2\,1/2}}{R} \quad (3)$$

where A, B, NEP and $i_n^{2\,1/2}$ denote the effective area (A = 1.35 × 10^{-4} cm^2), bandwidth, the noise equivalent power and the root-mean-square value of the noise current, respectively. The noise level at the bandwidth of 1 Hz was deduced to be ~2 × 10^{-14} A $Hz^{-1/2}$ by performing Fourier transformation of the dark current recorded at 10 V bias (Fig. S3, in Supporting Information). Therefore, the NEP was ~2.78 × 10^{-14} W $Hz^{-1/2}$. Accordingly, the value of D^* at 10 V bias was calculated to be ~4.18 × 10^{11} Jones. Note that such a decent D^* value was comparable with that of many previously reported β-Ga_2O_3 thin film-based DUV photodetectors [20,25,37]. Table 1 summarizes some important performance parameters of β-Ga_2O_3 thin film-based DUV photodetectors with MSM structure in literatures.

In addition to the incident light intensity, the operational bias voltage also had a great influence on the values of R and EQE. As shown in Fig. 5(a), both values rose progressively as the bias voltage increased. This was understandable because a larger external bias was helpful for accelerating separation of photocarriers and transfer of charge carriers, which would give a larger photoresponse. Further, the spectral response of our photodetector was studied, as plotted in Fig. 5(b). Evidently, the device exhibited a sizeable photoresponse in the DUV wavelength region from 200 to 280 nm with the peak response situated at ~250 nm. As the light wavelength increased, the photoresponse declined dramatically, rendering a sharp response cut-off edge at ~280 nm, which coincided with the optical absorption of the β-Ga_2O_3 thin films (Fig. 3(c)). What is more, the UV/visible rejection ratio defined as the ratio of responsivity at 250 and 400 nm (R_{250}/R_{400}), and the solar-blind rejection ratio defined as the ratio of responsivity at 250 and 300 nm (R_{250}/R_{300}) here were estimated to be ~1.45 × 10^3 and ~5.86 × 10^2, respectively. The results implied that the present β-Ga_2O_3 thin film-based DUV photodetector possessed an excellent solar-blind spectral selectivity.

The response speed that can reflect the capability of a photodetector to track quickly modulated photon signal was characterized as well. Fig. 5(c) displays a magnified photoresponse curve extracted from the time-dependent photoresponse, from which the rise and decay times (τ_r and τ_d) were deduced to be ~1.1 s and 0.03 s, respectively. Additionally, our photodetector also exhibited good reproducibility and stability. As depicted in Fig. 5(d), the time-dependent photoreponse could maintain almost unchanged with a good optical switching property even after thousands of cycles of operation. The slight fluctuation in photocurrent for each cycle was likely due to the disturbance existed in the measurement conditions. Furthermore, the air stability of our device was studied by re-measuring the time-dependent photoresponse after storage

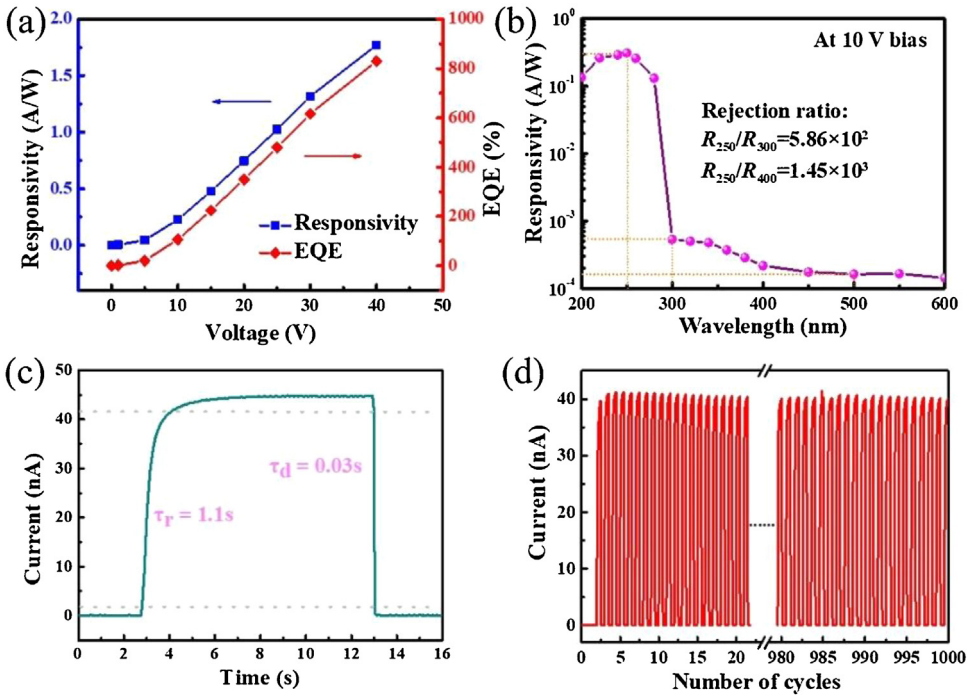

Fig. 5. (a) Responsivity and EQE of the device as functions of operational bias voltage. (b) Spectral responsivity of the device in the wavelength region of 200-600 nm. (c) An enlarged photoresponse curve shows the rise (τ_r) and decay times (τ_d). (d) Time-dependent photoresponse of the device over 1000 cycles of operation (265 nm, 0.952 mW cm^{-2}).

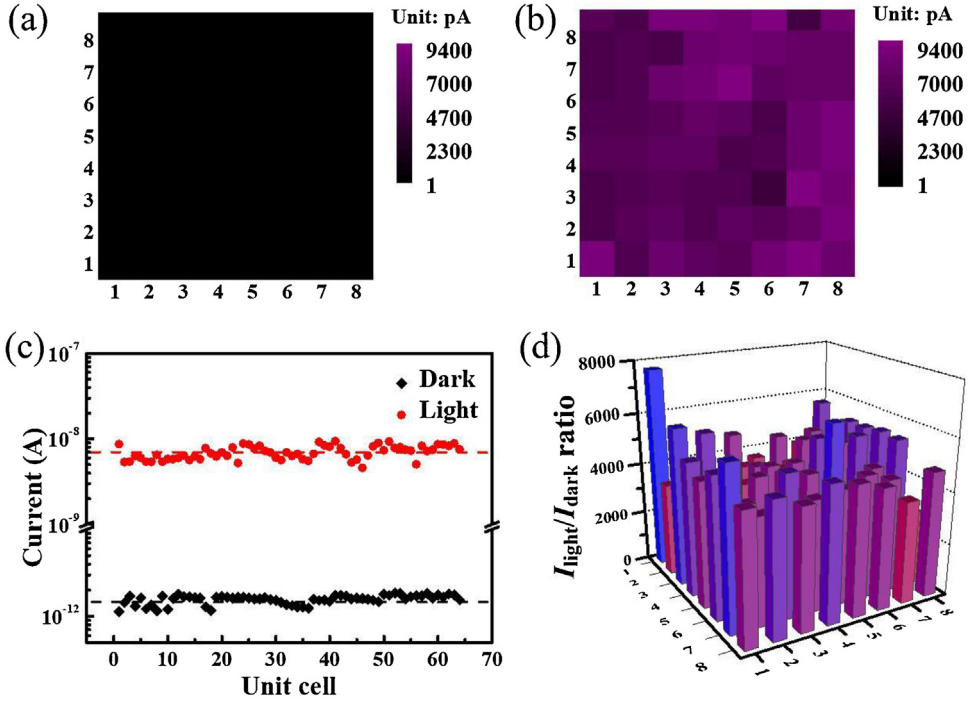

Fig. 6. 2D current contrast maps showing the channel currents of all the 8 × 8 devices (a) in dark and (b) upon 265 nm light illumination (0.25 μW cm^{-2}). (c) Channel current in dark and under 265 nm light irradiation for each device unit, the dash lines represent the average values for dark current (black) and photocurrent (red). (d) 3D diagram of the I_{light}/I_{dark} ratio for each device unit.

under ambient conditions without any protection for one month. As displayed in Fig. S4 (in Supporting Information), the device could kept its switching property and the photocurrent remained almost invariant, suggesting excellent air stability of the β-Ga_2O_3 thin film-based DUV photodetector.

In order to explore the possibility of the current β-Ga_2O_3 thin film-based photodetectors array for device integration application, the uniformity of the DUV photoresponse performance of all 8 × 8 device units was further probed. Here, the dark current and photocurrent under a homogenous 265 nm DUV irradiation (0.25

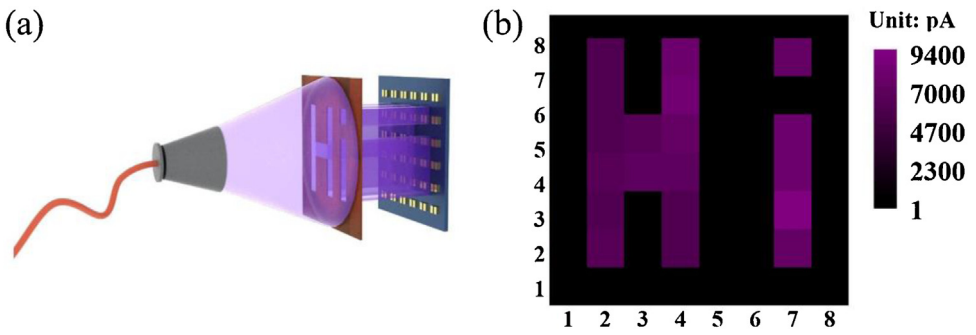

Fig. 7. (a) Schematic illustration of the setup for DUV light imaging. (b) The 2D current contrast map of the photodetectors array under 265 nm light illumination, showing the DUV light imaging function.

μW cm^{-2}) of each device were measured separately. For ease of comparison, the results were incorporated into 2D current contrast maps as demonstrated in Fig. 6(a) and (b), and the detailed data for all devices were provided in Fig. 6(c) as well. Obviously, these devices could operate properly. Careful analysis found that all device units had dark current in the range of 1–2 pA with an average value of ~1.57 pA, and photocurrent in the range of 5–9 nA with an average values of ~5.98 nA, at a bias of 10 V. The narrow fluctuations in both dark current and photocurrent suggested a uniform photoresponse performance. In addition, the I_{light}/I_{dark} ratio of all device units was extracted, which also showed a small fluctuation with the majority of the values in the range of 3×10^3-6 $\times 10^3$. Such a good uniformity of the device performance could be attributed to the small variation in the thickness of the patterned β-Ga_2O_3 thin films (Fig. S5 in Supporting Information), and also suggested a great potential for the present 8 × 8 device units for integrated device applications.

Finally, the ability of the β-Ga_2O_3 thin film-based photodetectors array to function as a DUV light image sensor was explored. As schematically shown in Fig. 7(a), a lab-built shadow mask with a pattern of "Hi" characters was placed between a homogenous 265 nm DUV illumination and the photodetectors array placed on a probe station. Only light illumination penetrating the hollow regime of the mask could shine on the devices while the rest of regimes were maintained in dark condition. While keeping the testing system still, the current of each device unit was recorded unit-by-unit by travelling a pair of probes connecting with a semiconductor parameter analyzer. After measurement of all units, the results were described by a 2D current contrast map. Significantly, as observed in Fig. 7(b), the shape of "Hi" could be clearly identified, which implied the preliminary DUV light imaging function of the β-Ga_2O_3 thin film-based photodetectors array. The spatial resolution could be further improved by means of increasing the number of the device units as well as reducing the size of each device unit.

Conclusion

In summary, we have demonstrated the periodic fabrication of high-quality β-Ga_2O_3 thin films by using a facile patterned technique. Especially, benefiting from the technique flexibility of standard photolithography, such a method could be applied to prepare patterned β-Ga_2O_3 thin films with arbitrary shapes in principle. With this technique, a β-Ga_2O_3-based photodetectors array comprising 8 × 8 device units was constructed, which showed excellent DUV photoresponse performance, in terms of a large Ilight/Idark ratio exceeding 10^4, a decent responsivity of ~0.72 A W^{-1}, and a specific detectivity of ~4.18×10^{11} Jones, respectively. In addition, the device could attain a large DUV/visible (250/400 nm) rejection ratio exceeding 10^3 with a steep response cut-off wavelength located at ~280 nm. What is more, the excellent uniformity and repeatability of the performance of the device units allowed the present photodetectors array to function as a DUV light image sensor with a reasonable spatial resolution. Given the ease of processing, low-cost and good compatibility with the well-developed techniques, the proposed method was believed to have a huge potential for β-Ga2O3-based integrated optoelectronic devices with multifunctional applications.

Acknowledgements

This work was supported by the National Natural Science Foundation of China (NSFC, Nos. 51902078, 62074048), the Fundamental Research Funds for the Central Universities (PA2020GDKC0014, JZ2020HGTB0051, JZ2018HGXC0001), and the Anhui Provincial Natural Science Foundation (2008085MF205).

Appendix A. Supplementary data

Supplementary material related to this article can be found, in the online version, at doi:https://doi.org/10.1016/j.jmst.2020.09.015.

References

[1] H. Chen, K. Liu, L. Hu, A.A. Al-Ghamdi, X. Fang, Mater. Today 18 (2015) 493–502.
[2] C. Xie, X.T. Lu, X.W. Tong, Z.X. Zhang, F.X. Liang, L. Liang, L.B. Luo, Y.C. Wu,Adv. Funct. Mater. 29 (2019), 1806006.
[3] L. Sang, M. Liao, M. Sumiya, Sensors 13 (2013) 10482–10518.
[4] E. Monroy, F. Omnes, F. Calle, Semicond. Sci. Technol. 18 (2003) R33–R51.
[5] Y.J. Lu, C.N. Lin, C.X. Shan,Adv. Opt. Mater. 6 (2018), 1800359.
[6] J.Y. Tsao, S. Chowdhury, M.A. Hollis, D. Jena, N.M. Johnson, K.A. Jones, R.J. Kaplar, S. Rajan, C.G. Van de Walle, E. Bellotti, C.L. Chua, R. Collazo, M.E. Coltrin, J.A. Cooper, K.R. Evans, S. Graham, T.A. Grotjohn, E.R. Heller, M. Higashiwaki, M.S. Islam, P.W. Juodawlkis, M.A. Khan, A.D. Koehler, J.H. Leach, U.K. Mishra, R.J. Nemanich, R.C.N. Pilawa-Podgurski, J.B. Shealy, Z. Sitar, M.J. Tadjer, A.F. Witulski, M. Wraback, J.A. Simmons,Adv. Electron. Mater. 4 (2018), 1600501.
[7] S.J. Pearton, J. Yang, P.H. Cary, F. Ren, J. Kim, M.J. Tadjer, M.A. Mastro, Appl. Phys. Rev. 5 (2018) 11301.
[8] D. Guo, Q. Guo, Z. Chen, Z. Wu, P. Li, W. Tang,Mater. Today Phys. 11 (2019), 100157.
[9] T.C. Wei, D.S. Tsai, P. Ravadgar, J.J. Ke, M.L. Tsai, D.H. Lien, C.Y. Huang, R.H. Horng, J.H. He, IEEE J. Sel. Top. Quantum Electron. 20 (2014) 112–117.
[10] J. Kim, S. Oh, M.A. Mastro, J. Kim, Phys. Chem. Chem. Phys. 18 (2016) 15760–15764.
[11] X. Chen, F. Ren, S. Gu, J. Ye, Photonics Res. 7 (2019) 381.
[12] W.Y. Kong, G.A. Wu, K.Y. Wang, T.F. Zhang, Y.F. Zou, D.D. Wang, L.B. Luo, Adv. Mater. 28 (2016) 10725–10731.
[13] D. Guo, Z. Wu, P. Li, Y. An, H. Liu, X. Guo, H. Yan, G. Wang, C. Sun, L. Li, W. Tang, Opt. Mater. Express 4 (2014) 1067.
[14] G.C. Hu, C.X. Shan, N. Zhang, M.M. Jiang, S.P. Wang, D.Z. Shen, Opt. Express 23 (2015) 13554.
[15] Y. Li, T. Tokizono, M. Liao, M. Zhong, Y. Koide, I. Yamada, J.J. Delaunay, Adv. Funct. Mater. 20 (2010) 3972–3978.
[16] C. Xie, X. Lu, M. Ma, X. Tong, Z. Zhang, L. Wang, C. Wu, W. Yang, L. Luo,Adv. Opt. Mater. 7 (2019), 1901257.
[17] Y. Qin, S. Long, H. Dong, Q. He, G. Jian, Y. Zhang, X. Hou, P. Tan, Z. Zhang, H. Lv, Q. Liu, M. Liu, Chin. Phys. B 28 (2019) 18501.

[18] D.Y. Guo, Z.P. Wu, Y.H. An, X.C. Guo, X.L. Chu, C.L. Sun, L.H. Li, P.G. Li, W.H. Tang, Appl. Phys. Lett. 105 (2014) 23507.
[19] X. Chen, K. Liu, Z. Zhang, C. Wang, B. Li, H. Zhao, D. Zhao, D. Shen, ACS Appl. Mater. Interfaces 8 (2016) 4185–4191.
[20] Y. Chen, Y. Lu, C. Lin, Y. Tian, C. Gao, L. Dong, C. Shan, J. Mater. Chem. C 6 (2018) 5727–5732.
[21] D. Guo, H. Liu, P. Li, Z. Wu, S. Wang, C. Cui, C. Li, W. Tang, ACS Appl. Mater. Interfaces 9 (2017) 1619–1628.
[22] B. Zhao, F. Wang, H. Chen, L. Zheng, L. Su, D. Zhao, X. Fang,Adv. Funct. Mater. 27 (2017), 1700264.
[23] B. Zhao, F. Wang, H. Chen, Y. Wang, M. Jiang, X. Fang, D. Zhao, Nano Lett. 15 (2015) 3988–3993.
[24] Y. Peng, Y. Zhang, Z. Chen, D. Guo, X. Zhang, P. Li, Z. Wu, W. Tang, IEEE Photon. Technol. Lett. 30 (2018) 993–996.
[25] Y.C. Chen, Y.J. Lu, Q. Liu, C.N. Lin, J. Guo, J.H. Zang, Y.Z. Tian, C.X. Shan, J. Mater. Chem. C 7 (2019) 2557–2562.
[26] Y. Chen, Y. Lu, M. Liao, Y. Tian, Q. Liu, C. Gao, X. Yang, C. Shan,Adv. Funct. Mater. 29 (2019), 1906040.
[27] J. Xu, W. Zheng, F. Huang, J. Mater. Chem. C 7 (2019) 8753–8770.
[28] Z. Galazka,Semicond. Sci. Technol. 33 (2018), 113001.
[29] L.M. Lin, Y. Luo, P.T. Lai, K.M. Lau, Thin Solid Films 515 (2006) 2111–2115.
[30] K. Sasaki, M. Higashiwaki, A. Kuramata, T. Masui, S. Yamakoshi, J. Cryst. Growth 392 (2014) 30–33.
[31] Q. Wang, J. Chen, P. Huang, M. Li, Y. Lu, K.P. Homewood, G. Chang, H. Chen, Y. He, Appl. Surf. Sci. 489 (2019) 101–109.
[32] A.P. Shah, A. Bhattacharya, J. Vac. Sci. Technol. A 35 (2017) 41301.
[33] Y. Zhang, A. Mauze, J.S. Speck, Appl. Phys. Lett. 115 (2019) 13501.
[34] X. Li, M. Zhu, M. Du, Z. Lv, L. Zhang, Y. Li, Y. Yang, T. Yang, X. Li, K. Wang, H. Zhu, Y. Fang, Small 12 (2016) 595–601.
[35] L. Wang, J. Jie, Z. Shao, Q. Zhang, X. Zhang, Y. Wang, Z. Sun, S.T. Lee, Adv. Funct. Mater. 25 (2015) 2910–2919.
[36] J.G. Hu, L.H. Zeng, M.Z. Wang, H. Hu, B. Nie, Y.Q. Yu, C.Y. Wu, L. Wang, C. Xie, F.X. Liang, L.B. Luo, ACS App. Mater. Interfaces 5 (2013) 9362–9366.
[37] M.Q. Li, N. Yang, G.G. Wang, H.Y. Zhang, J.C. Han, Appl. Surf. Sci. 471 (2019) 694–702.
[38] B.R. Tak, M. Garg, A. Kumar, V. Gupta, R. Singh, ECS J. Solid State Sci. Technol. 8 (2019) Q3149–Q3153.
[39] S. Rafique, L. Han, H. Zhao,Phys. Status Solidi 214 (2017), 1700063.
[40] A.S. Pratiyush, U.U. Muazzam, S. Kumar, P. Vijayakumar, S. Ganesamoorthy, N. Subramanian, R. Muralidharan, D.N. Nath, IEEE Photonics Technol. Lett. 31 (2019) 923–926.